The electronic states of isothiazole studied by VUV absorption spectroscopy and ab initio configuration interaction methods

ARTICLE *in* CHEMICAL PHYSICS · DECEMBER 2007

Impact Factor: 1.65 · DOI: 10.1016/j.chemphys.2007.09.044

2 AUTHORS, INCLUDING:

Michael H Palmer
The University of Edinburgh
311 PUBLICATIONS **3,365** CITATIONS

Available online at www.sciencedirect.com
ScienceDirect
Chemical Physics 342 (2007) 151–162
Chemical Physics
www.elsevier.com/locate/chemphys

The electronic states of isothiazole studied by VUV absorption spectroscopy and *ab initio* configuration interaction methods

Michael H. Palmer *, Agnieszka J. Gordon [1]

School of Chemistry, University of Edinburgh, West Mains Road, Edinburgh EH9 3JJ, Scotland, UK

Received 15 August 2007; accepted 22 September 2007
Available online 4 October 2007

Abstract

The isothiazole VUV absorption spectrum over the range 5–12 eV shows (broad) intense bands centred near 5.17, 6.11, 7.37, 7.75, 9.18 and 10.43 eV. The lowest Rydberg states relating to the first ionisation energy are difficult to identify, but higher members are particularly numerous on the region from 8.4 to 9.6 eV. Electronic excitation energies for valence (singlet and triplet) and Rydberg-type states have been computed using *ab initio* multi-reference multi-root CI methods. These studies used a triple zeta + double polarisation basis set, augmented by diffuse (Rydberg) orbitals. The theoretical study shows the nature of the more intense Rydberg state types, and positions of the main valence and Rydberg bands. By study of the excitation energies to specific upper states, the vertical ionisation energies (IE) are confirmed as $\pi_4^{-1} < \pi_3^{-1} < \sigma_{18}^{-1}(LP_N) < \sigma_{17}^{-1}(LP_S)$. Structures for the π- and σ-cations, and the (neutral) ππ*-triplet states have been obtained. Calculated energies for low-lying Rydberg states are close to those observed, and there is generally a good correlation between the theoretical intensities and the experimental envelope. The ground state atomic and molecular properties are in good agreement with experiment.

Keywords: Vacuum UV absorption; Rydberg states; Valence states; Triplet states; CI calculations; Ionisation potentials; Excited state structures

1. Introduction

Ultraviolet (UV) spectroscopy was the first of the spectroscopic techniques; however, it has proved to be one of the most difficult for detailed interpretation, owing to major computational requirements. Hence there remains a challenge for this type of study, especially for molecules where a number of differing excitation processes are possible. We have previously reported a series of joint experimental and theoretical studies of the UV + vacuum-UV (VUV) spectra of the 5-membered ring heterocycles shown in Fig. 1; these include furan (**1a**) [1], pyrrole (**1b**) [2,3], thiophene (**1c**) [4,5], pyrazole (**2b**) [6,7], isoxazole (**2a**) [8], oxazole (**3a**) [9] and very recently thiazole (**3c**). We now report a study of the VUV spectrum of isothiazole (**2c**), one of the least well-known members. There are relatively few isothiazoles in nature, but recently 5,5′-diphenyl-3,3′-diisothiazole disulfide has been shown to have antipoliovirus activity [10]. We include a large scale CI study of the electronically excited (singlet and triplet) valence and Rydberg states, to provide guidance over the assignment. We have also reinvestigated the order of cationic states in the UV-photoelectron spectrum (UV-PES) [11], since this is fundamental to determination of the sequence of Rydberg states.

1.1. Electronic structure of the ground state

The doubly occupied SCF orbitals for the $\widetilde{X}^1$ A′ ground state (C_s symmetry) of isothiazole [11] (shown in its inertial axis system in Fig. 2) are: 1a′–18a′ (σ-electrons), 1a″–4a″ (π-electrons); 17a′ and 18a′ are dominated by density on S and N, respectively, and are designated as LP_S and LP_N, respectively, where LP stands for lone pair. The com-

* Corresponding author. Tel.: +44 0 131 650 4765.
E-mail address: m.h.palmer@ed.ac.uk (M.H. Palmer).
[1] On leave of absence from Faculty of Chemistry, University of Wroclaw, Poland.

0301-0104/$ - see front matter © 2007 Elsevier B.V. All rights reserved.
doi:10.1016/j.chemphys.2007.09.044

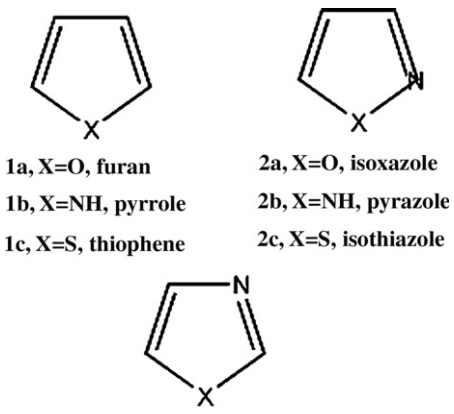

Fig. 1. The azole series of molecules.

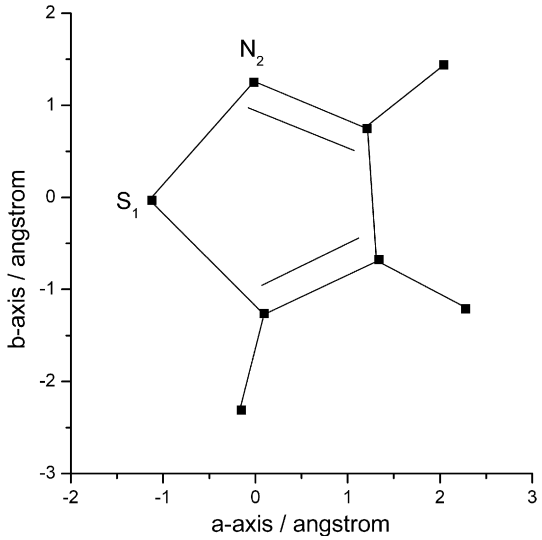

Fig. 2. Isothiazole lying in the inertial axis system.

bined a′ and a″ (σ/π) sequence is discussed below. In all the CI results described here for isothiazole, the core (1a′–8a′ + 1a″) is frozen at 2.0 e for each MO.

1.2. Molecular structure of isothiazole

The ground state rotational (A_0, B_0, C_0) and quartic centrifugal distortion constants, have been determined by microwave [12–14] and high resolution infrared spectral (IR) studies [15]. An electron diffraction (ED) study [16] has been reported, which combined ED and MW data [12], to generate a consistent structure.

Molecular properties from the MW studies, including dipole moments [12,13], ^{14}N quadrupole coupling constants [13,14], are compared with our ground state structural results in Appendix A below; these ground state theoretical results complete the picture of ground and excited state properties, and also give a measure of the reliability of the present ground state wave-function for the excited state study.

1.3. Assignment of the ionisation energies (IE_V) from the UV-PES spectrum

A UV-PES study of isothiazole [11], gave an assignment of ionisation energies (IE) based upon orbital energies (Koopmans' Theorem, KT); the order of the four lowest IE's were: $\pi_4^{-1} < \pi_3^{-1} < \sigma_{18}^{-1} < \sigma_{17}^{-1}$. Only IE_1 is well resolved with IE_A (adiabatic) 9.65 eV. IE_2 and IE_3 overlap, with estimated IE_V 10.35 and 10.90 eV, while IE_4 is significantly higher at 12.50 eV [11].

The Rydberg formula *is* $IE_A - E = R/(n-\delta)^2$, where R is the Rydberg constant (13.606 eV), n is the principal quantum of the upper (Rydberg) orbital, and δ is the quantum defect. The four IE above [11] should show Rydberg 3s states (for $n = 3$, $\delta = \sim 1$) at energies of ~6.25, ~6.95, ~7.5 and ~9.1 eV, so all of these IE will contribute to the VUV envelope in the present range below 12 eV.

2. Experimental methods

The present description supplied by the Daresbury Laboratory [17], where the measurements were performed, is reproduced in Appendix B; this includes techniques to reduce thermal transpiration effects between the absorption cell and the sensor assembly, in order to be certain that the correct sample pressure was recorded [18,19]. The spectral sample (Aldrich) had no additional infrared bands to those reported in the literature.

A wide scan VUV spectrum is shown in Fig. 3, and the principal assigned lines are shown in Table 1. Expanded regions of the spectrum are shown in Figs. 4 and 5. Absorption bands arising from excitation of a pure Rydberg state are expected to exhibit the vibrational structure of the UV-PES, and were identified by this means. IE_1 showed [11] a complex vibrational progression of at least

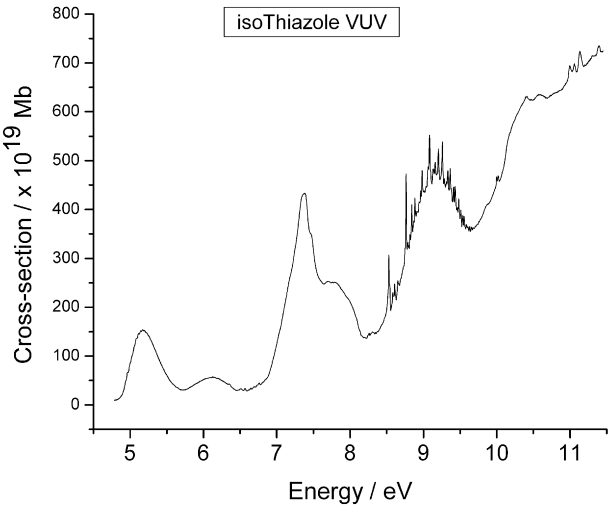

Fig. 3. The VUV spectrum of isothiazole.

Table 1
Observed structure in the valence and Rydberg states of isothiazole

Valence state		Rydberg states limit IP_1 9.65 eV						
	Energy/eV	Assignment		Energy/eV				
0–0	**4.908**	**s-series**	n	0–0	υ_2	υ_3	$2\upsilon_2$	υ_4
υ_1	4.937	$\delta = 1.08$	5	8.763	8.815	8.840	8.867	8.885
$2\upsilon_1$	4.965		6	9.084	9.134	9.160	9.205	9.259
$3\upsilon_1$	4.993		7	9.259	9.332	9.380		9.465
$4\upsilon_1$	5.020		8	9.363				
$5\upsilon_1$	5.052		9	9.432				
$6\upsilon_1$	5.083		10	9.481				
$7\upsilon_1$	5.114		11	9.510				
$8\upsilon_1$	5.142		12	9.535				
$9\upsilon_1$	5.169		13	9.554				
$10\upsilon_1$	5.195	**p-series**	4	8.528	8.582	8.607		8.650
$11\upsilon_1$	5.230	$\delta = 0.48$	5	8.981	9.034			
$12\upsilon_1$	5.259		6	9.204		9.283		
$13\upsilon_1$	5.285		7	9.333				
			8	9.412				
			9	9.462				
		p′-series	4	8.541				
		$\delta = 0.50$	5	8.982		9.044	9.063	9.108
		d-series	4	8.764				
		0.08						

Vibrational satellites have υ_1, υ_2, υ_3 and υ_4 28, 53, 77 and 120 meV, respectively.

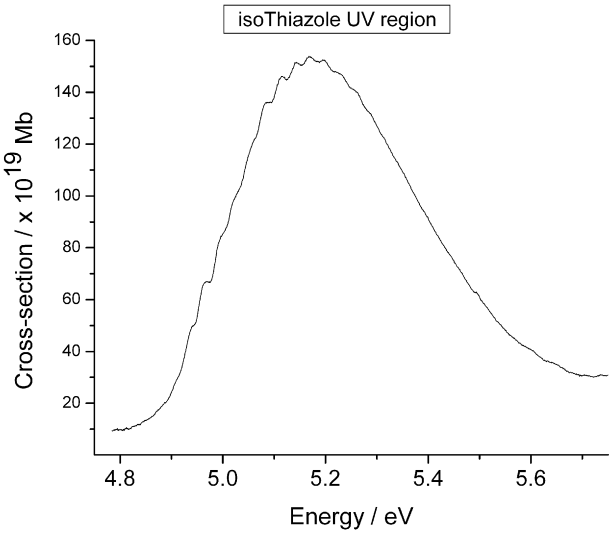

Fig. 4. Expanded region of the UV spectrum of isothiazole.

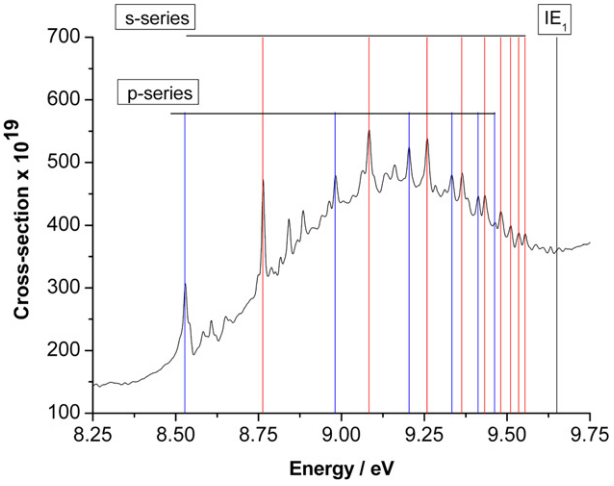

Fig. 5. Assigned Rydberg states in the VUV spectrum of isothiazole.

eight members where the adiabatic (IE_A) and vertical (IE_V) ionisation energy coincide at 9.65 eV [11]. A strong 0–0 band implies a π-ionisation (here π_4^{-1}) [1–10]; we make extensive use of this envelope for the Rydberg study. The UV-PES is superimposed on the VUV as either a partial spectrum, or stick diagram (Figs. 6 and 7).

3. Theoretical Methods

3.1. Basis sets

The main theoretical parts of the present study employed a triple-zeta valence with polarisation basis set (TZVP; e.g., S[6s5p2d} contracted functions) [21,22]. These were augmented with a 4s3p3d set of centre-of-mass-based Rydberg functions leading to overall acronym TZVPR. The exponents were: s-type 0.021, 0.008, 0.0025, 0.0008; p-type 0.017, 0.009, 0.004; d-type 0.015, 0.008, 0.004; these closely match our previous work [1–8]. This basis set is flexible enough to study electronically excited states of valence and Rydberg character for molecules of this type over an energy range up to about 14 eV [1–8], and has proved to be slightly superior [9,10] to cc-pVTZ, which has one less valence AO, but additional polarisation.

3.2. Structures

The isothiazole molecule (C_S symmetry) lies in the x,y-plane. All CI calculations were performed at the $\widetilde{X}^1$ A′

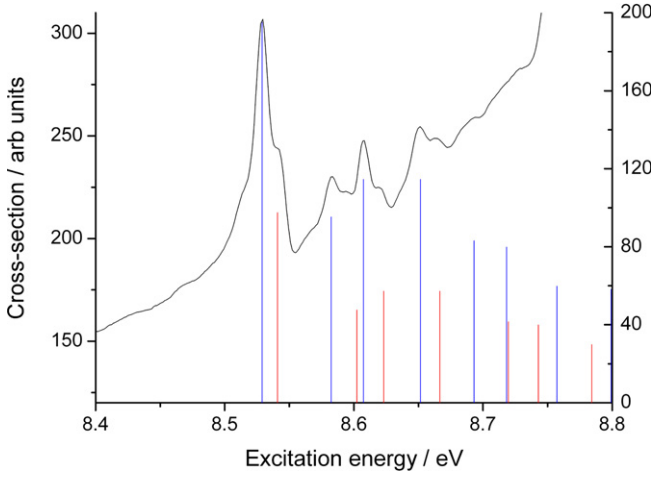

Fig. 6. Superimposed VUV and UV-PES spectra of isothiazole in the 8.5–8.8 eV region.

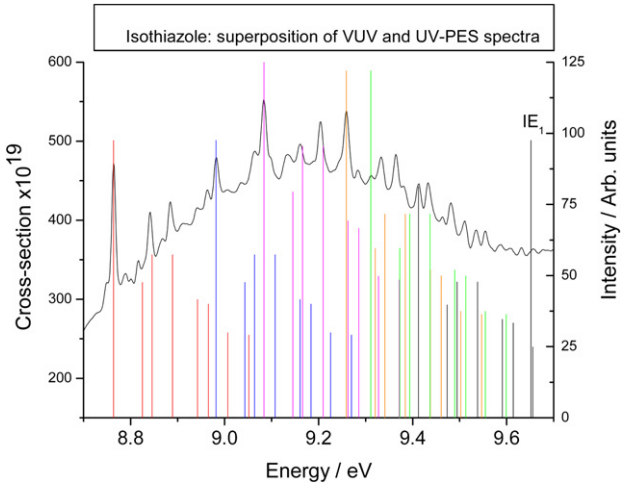

Fig. 7. Overlay of the VUV and UV-PES spectra in the 8.8–9.6 eV region.

ground state (TZVP + MP2) equilibrium geometry, which shows good agreement with the molecular properties from the MW study [12] (see Appendix A). We have determined structures for two C_S symmetry cationic states ($\widetilde{B}^2A'$ and $\widetilde{X}^2\ A''$) and the lowest triplet state ($\tilde{a}_3A'$) of isothiazole (both C_S and C_1 symmetry), using UHF-B3LYP methods; the corresponding UHF-MP2 optimizations were extremely slow, and offered no additional information. The equilibrium structure of the lowest cation was readily obtained, and was found to be planar ($\widetilde{X}^2A''$); attempts to generate the ($\widetilde{A}^2A''$) were unsuccessful owing to collapse to $\widetilde{X}^2A''$. Use of the 'swap + lock' techniques in GAMESS-UK [23] then enables the corresponding structure of the $\widetilde{B}^2A'$ cation to be obtained. In the case of the planar $\pi\pi^*$-triplet state, an imaginary vibration frequency occurs, which becomes positive by relaxation to C_1 symmetry.

The vertical IEs were also studied by MRD-CI, Green's Function (GF) and non-diagonal Tamm-Dancoff Approximation (TDA) methods at the TZVP + MP2 equilibrium structure; the results are shown in Table 2.

3.3. Multi-reference CI calculations

These computations were performed with the multi-reference multi-root configuration interaction (MRD-CI) module [24–27] in GAMESS-UK [23]. The upper limit of main reference configurations (CSFs) used in the CI module is 180 spin combinations of two and four open-shell types; these are expanded up to eight open shells at the CI stage by single and double excitations. The largest calculations performed, generated in excess of 10^8 CSFs.

3.3.1. Treatment of valence and Rydberg states

Mulliken analysis of the TZVPR virtual MOs (VMOs) enabled these to be divided into subgroups for the Rydberg state study. For simplicity, we denote p_x-, d_{xz}-states, etc. as X and XZ, etc. Most of the VMOs are almost pure single types, but some mixing occurs between the sets (X^2–Y^2), XY and ($3Z^2$–R^2). Although there is no strict separation of *either* X and Y, *or* XZ and YZ, etc. in C_S symmetry, it proved possible to perform a series of separate CI studies.

The final reference configurations (CSF) were built up in stages by recycling CSF which emerge with density $\geqslant 10^{-5}$e from cycle N of the CI, into the reference set in cycle $(N+1)$; this was repeated until the output wave-functions for each electronic state contained no new CSF. Considerable care is needed to generate a satisfactory set of reference CSFs [1–8], since some CSF with 4-open shells and other double excitation types, have ~1 eV effect on the excitation energy [28]. The principal types of 'excited' CSF are those with *either* (a) simultaneous excitation of a further $\pi\pi^*$ type, *together with* the existing primary π- or σ-excitation, *or* (b) double vacation of the occupied

Table 2
Vertical cationic states (eV) for isothiazole compared with UV-PES spectra

Sym.	Open shells	CI		Green's function		Tamm Dancoff (nondiagonal) approximation		Exptl. IP_V/eV [11]
		IP	Density (c_i^2)	IP	Pole strength	IP	Pole strength	
$^2A''$	π_4^1	9.712	0.839	9.323	0.922	9.236	0.903	9.77
$^2A''$	π_3^1	9.978	0.837	9.762	0.910	9.602	40.881	10.35
$^2A'$	$(18a')^1$	10.428	0.815	11.085	0.907	10.962	0.884	10.90
$^2A'$	$(17a')^1$	12.548	0.829	12.383	0.921	12.417	0.909	12.50
$^2A''$	π_2^1	12.864	0.710	14.445	0.915	13.224	0.677	
$^2A'$	$(16a')^1$	13.345	0.797	13.671	0.824	14.308	0.892	13.55
$^2A'$	$(15a')^1$	13.202	0.793	14.366	0.907	14.528	0.894	

π-MOs (especially the HOMO, π_4) into $\pi_5^*\pi_6^*$ and/or σ^* VMOs.

The intensity of the transitions, is determined here by the theoretical oscillator strength $f(r)$; for Rydberg states this is typically 10^{-2}–10^{-6}, while for valence states $f(r)$ it is typically 0.8–10^{-2}. As well as excitation energy, we use the total CI values of the second moments of the charge distribution ($\langle x^2\rangle$, $\langle y^2\rangle$, $\langle z^2\rangle$), as measures of the nature of the state, valence or Rydberg. These terms vary markedly from near −20 a.u. for valence natural orbitals (NOs) to near −500 a.u. for 5s and related states, and relatively specific angular distribution for X, Y, Z, etc.

4. Results

4.1. Experimental VUV absorption

The overall envelope of the isothiazole VUV absorption (Fig. 3) shows broad bands with maxima near 5.2 and 6.1 eV, a complex envelope with maxima near 7.4 and 7.8, and further bands near 9.1 and 10.3 eV. These bands are expected to contain valence transitions, some of which have high calculated values for $f(r)$, as discussed below.

The 5.18 eV band shows (Fig. 4) a progression on the leading edge of at least 13 members, with a separation of 0.029 eV (234 cm^{-1}), and no apparent anharmonicity (Table 1); this value is sufficiently low to present a dilemma, namely whether a rotational or vibrational effect is responsible. The (recently analysed [15,16]) lowest IR band (υ_{18}, A″) has band centre at 478.6 cm^{-1}, twice this VUV band separation. Although we have been unable to determine the structure, or perform a vibrational analysis for the lowest singlet state of isothiazole, we do have the results for the triplet state (Sections 3.2 and 4.2), which shows that the triplet has a lowest frequency of 263 cm^{-1}. We assume that the observed VUV progression (234 cm^{-1}) is the corresponding vibrational interval of the singlet.

The second band of the VUV spectrum at 6.1 eV is broad, with very weak features. A series of bands at higher energy (Table 1), readily fit an s-series (8.763 eV, for $n = 5$), where $\delta = 1.08$ (Fig. 5). Extrapolation gives the 3s member ~5.946 eV; the strong 6.1 eV broad band does contain a series of minor undulations, which fit with the first member at 5.95 eV, but this is not convincing. The weak, but relatively sharp structure lying near 6.565 eV, gives a more convincing fit for a Rydberg state, but is not readily interpreted, unless the vibrational structure (not resolved in the UV-PES) is similar for IE_1 and IE_2, in which case the 6.565 eV band is the 3s state of the latter.

The np-series (Table 1) with $\delta = 0.48$ (Fig. 5), gives an extrapolated value for the 3p member of 7.759 eV, but there is no evidence of this electronic state with the present VUV spectrum.

At 8.53 eV, the vibrational structure of the VUV and the UV-PES IE_1 band envelope clearly are identical (Fig. 6); this identifies a Rydberg state with $n - \delta = 3.485$, from which $n = 4$ and $\delta = 0.515$, a 4p type state. All the bands of the VUV in this region appear doubled (Fig. 6), with a weaker set ~100 cm^{-1} to higher energy; we provisionally assign these to a second Rydberg state (4p′). Above this energy, several other sets of VUV bands which exhibit the UV-PES vibrational structure are evident, as shown in Fig. 7 and summarised in Table 1.

4.2. Theoretical results

The equilibrium structures of the lowest lying cationic states are compared with the ground and ππ*-triplet states in Fig. 8. The calculated cationic states for vertical ionisation of isothiazole are shown in Table 2. The principal theoretical results for the singlet valence states for thiazole showing vertical excitation energies (eV), oscillator strengths, and second moments (a.u.) are shown in Tables 3 (singlets) and 4 (triplets). Similarly, the calculated sequential singlet Rydberg states for thiazole are shown in Table 5, and the comparison of ground state molecular properties with MW results in Table 6. Only differences from the SCF configuration σ_1^2–$\sigma_{18}^2\pi_1^2$–π_4^2 are shown for the excited states in Tables 3–5.

4.2.1. Adiabatic structures

Both the optimized equilibrium and ED structure [16] of isothiazole are considerably distorted (Fig. 8a and b) from a regular pentagon, with (calculated) ring angles differing

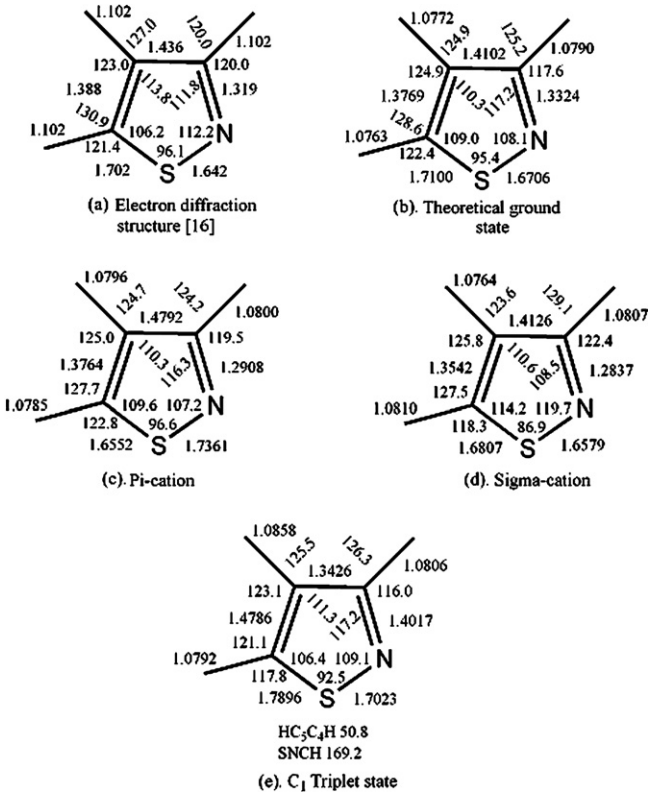

Fig. 8. Comparison of adiabatic structures for the ground, triplet and cationic structures, and the electron diffraction structure.

Table 3
Sequential singlet valence states for isothiazole; vertical excitation energies[a] (eV), oscillator strengths and second moments (a.u.)

Energy/eV	State	Excitation	$10^6 f(r)$	$\langle x^2\rangle$	$\langle y^2\rangle$	$\langle z^2\rangle$
0	$\tilde{X}^1A'$	$1-18\sigma^2\pi_1^2\pi_2^2\pi_3^2\pi_4^2$		−26.8	−24.2	−28.9
5.312	A′	$\pi_4\pi_5^*+\pi_3\pi_6^*$	208,573	−28.9	−23.9	−29.4
5.911	A″	$LP_N\pi_5^*-LP_N\pi_6^*$	5702	−24.1	−26.2	−31.0
6.443	A′	$\pi_3\pi_5^*-\pi_4\pi_6^*$	124,363	−27.0	−26.3	−27.8
6.640	A′	$LP_N\sigma_{20}^*+LP_N\sigma_{19}^*+\pi_4\pi_7$	46,971	−35.7	−32.9	−31.7
6.665	A″	$\pi_3\sigma_{20}^*-\pi_3\sigma_{19}^*$	704	−27.5	−30.6	−28.4
6.791	A″	$\pi_4\sigma_{19}-\pi_4\sigma_{20}^*$	803	−29.6	−27.5	−27.9
7.586	A′	$\pi_3\pi_6^*+\pi_2\pi_5^*$	227,280	−27.0	−27.6	−30.2
7.648	A′	$LP_N\sigma_{20}^*-LP_N\sigma_{19}^*+\pi_3\pi_6^*$	147,286	−24.8	−30.8	−29.9
7.857	A′	$\pi_4\pi_6^*+\pi_3\pi_5^*$	279,248	−29.9	−25.3	−30.2
7.869	A″	$LP_S\pi_5^*$	12,887	−28.9	−21.2	−30.9
7.999	A″	$LP_N\pi_7^*+LP_N\pi_6^*$	1876	−24.8	−27.7	−31.8
8.704	A″	$\sigma_8\pi_5^*$	1973	−27.5	−22.2	−31.1
8.738	A″	$\pi_4\sigma_{20}^*+\pi_4\sigma_{19}^*$	8730	−38.5	−35.5	−29.4
8.757	A″	$\pi_4\sigma_{21}^*-\pi_4\sigma_{23}^*$	5	−38.9	−30.4	−28.6
9.180	A″	$\pi_4\sigma_{22}-\pi_4\sigma_{23}^*$	3040	−39.6	−37.4	−28.9
9.183	A″	$\pi_3\sigma_{21}^*+\pi_3\sigma_{19}^*-\pi_3\sigma_{20}^*$	6181	−37.9	−35.8	−28.9
9.373	A′	$\pi_2\pi_5^*-\pi_3\pi_6^*-\pi_3^0\pi_5^{2*}$	109,349	−28.2	−25.8	−30.1
9.455	A″	$\pi_3\sigma_{19}+\pi_3\sigma_{20}^*$	9077	−38.7	−35.3	−29.6
9.592	A′	$\pi_3\pi_4^{2*}-\pi_3\pi_7^*+\pi_3\pi_6^*-\pi_3^0\pi_5^{2*}$	36,611	−27.8	−26.3	−34.8
9.620	A″	$\pi_4\sigma_{23}^*+\pi_4\sigma_{21}^*$	33,994	−36.0	−31.7	−29.2
9.751	A′	$\pi_3\pi_4\pi_5^{2*}-\pi_3\pi_7^*+\pi_4\pi_7^*-\pi_4^0\pi_5^{2*}$	25,662	−28.3	−26.1	−32.5
10.804	A′	$LP_S\sigma_{20}^*-LP_S\sigma_{19}^*$	275,179	−29.2	−26.4	−30.0
11.037	A′	$\pi_3\pi_7^*-\pi_4\pi_7^*-LP_N\sigma_{19}^*-\pi_3\pi_4\pi_5^{2*}$	8325	−30.3	−25.1	−35.6

[a] Excitation energies are relative to the $^1A'$ energy −568.075001 a.u.

Table 4
Sequential triplet valence states for isothiazole; vertical excitation energies[a] (eV) and second moments (a.u.)

Energy/eV	State	Type	$\langle x^2\rangle$	$\langle y^2\rangle$	$\langle z^2\rangle$
4.113	A′	$\pi_4\pi_5^*$	−26.3	−26.3	−29.5
4.401	A′	$\pi_3\pi_5^*$	−29.5	−23.2	−29.2
5.419	A″	$LP_N\pi_5^*$	−23.9	−26.3	−31.0
6.141	A″	$\pi_4\pi_6^*$	−29.3	−25.0	−29.9
6.157	A″	$\pi_4\sigma_{19}^*-\pi_4\sigma_{20}^*$	−30.2	−28.1	−28.0
6.483	A″	$\pi_3\sigma_{20}^*-\pi_3\sigma_{19}^*$	−27.1	−32.0	−28.6
7.345	A′	$\pi_3\pi_6^*-\pi_2\pi_5^*$	−27.5	−26.9	−29.8
7.664	A″	$LP_S\pi_5^*$	−29.0	−21.1	−30.9
7.928	A′	$LP_S\sigma_{19}^*-LP_S\sigma_{20}^*$	−29.6	−25.1	−29.5
7.954	A″	$LP_N\pi_6^*+LP_S\pi_5^*$	−24.8	−27.7	−31.8
8.219	A′	$\pi_2\pi_5^*+\pi_3\pi_6^*$	−27.9	−26.1	−29.8
8.452	A″	$\pi_4\sigma_{19}^*+\pi_4\sigma_{20}^*$	−41.1	−32.3	−29.5

[a] Excitation energies are relative to the $^1A'$ energy −568.075001 a.u.

from 108° by maximal values of −13° (at S) and +9° (at C_3). The ring bond lengths have $C_3N_2 < C_5C_4 < C_4C_3 \ll SN_2 < SC_5$. Both the MW [32] and ED [16] structures shows the same bond length sequence, although the present CH are shorter than the ED by 0.025 Å, and the CC and CN also differ by ~0.025 Å; owing to insufficient isotopomers being studied, the MW studies [32] are insufficient for a full substitution structure.

The π-cation (Fig. 8c) with C_S symmetry is the lowest cation, shown by starting with a non-planar C_1 structure, which optimizes to C_S with all positive vibration frequencies; it has C_5–S_1 and C_3–N_2 shortened by 0.05 and 0.04 Å, while S_1–N_2 and C_3–C_4 are lengthened by 0.06 and 0.07 Å, respectively; C_4–C_5 and C–H and all angles are relatively unchanged. This implies a weakening of the S_1–N_2 bond and reduced conjugation of the buta-1,3-diene moiety N_2–C_3–C_4–C_5. Nearly 60% of the total charge in the π-cation is derived from S_1 (37%) and C_3 (20%), with much less from the other centres, with N_2 effectively unchanged.

In contrast, the σ-cation (Fig. 8d has bond lengths shortened by only ~0.02–0.03 Å, but all ring angles (except C_4) are changed, with S_1 being closed (5°) and both C_5 and N_2 being opened (10°), respectively. The cationic charge is removed from C_3 (22%), N_2 (21%), S_1 (18%) and each H (12%).

The planar ππ*-triplet state (excitation energy 4.171 eV) structure (Fig. 8e) shows major differences from the other three structures. Both SN and SC bonds are lengthened significantly; the angles at C_3 and C_4 are opened, and the alternating C=C–C=C representation of the ground state is replaced by the C–C=C–C unit. Thus the structure of the lowest triplet is very close to the excited state of cis-butadiene, where the π_3^* MO is singly occupied, and a non-planar system seems probable. Indeed, the isothiazole ππ*-triplet state ($^3A'$) shows a negative vibration frequency (υ_{18}, −162 cm^{-1}), which became positive (263 cm^{-1}) when the structure was relaxed to C_1 symmetry under B3LYP conditions; the S^2 operator was 2.0117 under these latter conditions. In both C_S and C_1 structures, the atomic motion of υ_{18} is dominated by H_5 out-of-plane bending. The C_1 symmetry triplet is essentially planar, except for the S and H_5 atoms which lie on opposite sides of the plane. The dihedral angles $S_1N_2C_3C_4$ and $H_4C_4C_5H_5$ are 13.4° and 50.8°, respectively, showing a marked twist of the latter

Table 5
Sequential singlet Rydberg states for isothiazole, vertical excitation energies[a] (eV), oscillator strengths and second moments (a.u.)

Energy/eV	Symmetry	Excitation type	10^6 $f(r)$	$\langle x^2\rangle$	$\langle y^2\rangle$	$\langle z^2\rangle$
6.282	A″	π_4S	70	−84.3	−59.2	−59.4
6.757	A″	π_3S	5637	−86.0	−65.1	−63.2
7.329	A″	π_4Y	30,873	−65.8	−84.7	−52.3
7.701	A″	π_3Y	3108	−60.1	−82.9	−50.9
7.728	A″	π_4X	1322	−86.1	−89.1	−71.9
7.811	A′	π_4Z	2768	−61.9	−50.8	−123.2
7.937	A′	π_4YZ	5769	−81.0	−121.9	−148.6
7.990	A′	σ_{18}S	21,216	−72.5	−54.9	−54.4
8.060	A″	π_4S	818	−293.0	−258.2	−246.3
8.166	A″	π_3X	39	−90.0	−95.7	−77.3
8.178	A″	π_4XY	819	−102.3	−67.9	−67.1
8.194	A′	π_4XZ	476	−98.3	−61.8	−126.7
8.194	A″	π_4Y	18,239	−100.3	−144.4	−75.2
8.209	A″	π_4X	16,485	−81.0	−59.7	−57.3
8.237	A″	π_4S	5223	−125.2	−110.4	−124.7
8.289	A″	σ_{18}Z	12,795	−44.4	−33.7	−65.9
8.294	A′	π_3YZ	3737	−93.2	−154.5	−182.8
8.444	A′	π_4Z	66,869	−111.9	−93.6	−245.2
8.463	A′	π_4YZ	34,948	−110.1	−167.7	−204.9
8.484	A″	π_3X	24	−87.8	−94.1	−75.5
8.491	A″	π_3S	1370	−128.5	−118.9	−131.0
8.515	A′	π_4XZ	15,135	−79.4	−50.4	−110.4
8.525	A″	π_3XY	3946	−104.3	−70.5	−69.3
8.542	A″	π_3Y	10	−95.0	−145.2	−74.6
8.547	A″	π_4XY	3882	−161.8	−92.1	−76.1
8.614	A′	π_3XZ	4725	−84.6	−57.9	−117.3
8.615	A′	σ_{18}Y	2326	−61.2	−88.7	−54.5
8.627	A′	π_4YZ	4668	−60.1	−109.3	−109.3
8.775	A″	π_3X	33,127	−79.5	−61.9	−57.8
8.776	A″	σ_{18}Z	3631	−54.6	−52.7	−121.1
8.804	A′	π_3YZ	60,903	−58.8	−91.3	−109.8
8.834	A′	σ_{18}X	10,709	−74.8	−62.2	−59.2
8.848	A″	σ_{18}YZ	1	−61.0	−94.2	−116.6
8.862	A′	σ_{18}X	1050	−86.9	−95.9	−79.2
8.870	A″	π_4X	117	−273.6	−232.1	−186.3
8.882	A″	π_3XY	30	−155.9	−94.5	−74.9
8.898	A′	σ_{18}XY	8837	−159.5	−82.0	−87.4
8.908	A′	π_4Z	25,259	−139.1	−123.7	−335.8
8.956	A′	π_3XZ	7001	−94.6	−61.3	−126.3
8.973	A′	π_4XZ	5543	−241.1	−142.2	−298.1
9.028	A″	π_4XY	8168	−89.4	−74.5	−53.2
9.080	A′	π_3Z	54,772	−60.5	−55.4	−127.8
9.088	A″	π_3X	0.0	−265.3	−230.5	−181.2
9.265	A″	σ_{18}XZ	611	−59.9	−45.4	−98.7
9.271	A′	π_2Z	27,830	−43.5	−31.0	−56.1
9.308	A′	π_3YZ	20,187	−109.4	−186.9	−218.9
9.386	A″	π_4Y	3245	−154.6	−260.7	−117.0
9.392	A′	π_3XZ	944	−237.0	−143.4	−295.1
9.459	A″	π_3XY	731	−83.3	−74.6	−52.3
9.484	A′	σ_{18}Y	3648	−99.1	−152.8	−79.1
9.515	A″	σ_{18}YZ	895	−70.8	−134.3	−153.6
9.685	A″	σ_{18}XZ	23	−114.1	−74.2	−147.7
9.699	A′	σ_{18}S	13,887	−111.9	−97.8	−103.7
9.824	A′	σ_{18}X	24	−256.9	−223.5	−175.6
9.872	A″	σ_{18}Z	2178	−109.1	−93.3	−242.5
9.922	A″	σ_{18}YZ	28	−122.2	−202.9	−244.0
9.926	A′	σ_{17}S	45,908	−75.3	−48.2	−52.5
9.947	A″	π_3Y	41	−157.7	−271.0	−120.4
10.031	A″	π_4S	50	−471.9	−441.4	−449.0
10.211	A′	π_4Z	356,508	−71.2	−60.7	−146.0
10.313	A′	π_2XZ	7768	−134.1	−88.7	−171.4
10.321	A″	σ_{18}Z	6859	−80.5	−73.1	−180.9
10.441	A′	σ_{18}S	112	−521.1	−508.5	−221.2
10.450	A′	σ_{18}Y	1368	−145.5	−257.8	−116.4
10.533	A′	σ_{17}Y	5066	−62.8	−78.8	−52.5
10.539	A″	σ_{18}XZ	10	−237.0	−146.3	−302.7
10.639	A′	σ_{17}X	12,082	−92.6	−91.4	−79.3
10.752	A′	σ_{18}XY	10,224	−87.7	−80.4	−56.6
10.771	A″	σ_{17}Z	535	−63.8	−48.0	−124.7
10.897	A″	σ_{17}YZ	5701	−64.0	−87.2	−113.7
10.914	A′	σ_{179}XY	21,039	−167.3	−78.6	−89.5
10.969	A″	π_2Y	3610	−63.2	−84.4	−51.5
11.069	A′	π_2XZ	5067	−85.8	−57.0	−117.5
11.130	A′	π_2YZ	131	−46.5	−62.8	−76.2
11.135	A″	σ_{17}XZ	585	−64.4	−40.2	−98.2
11.247	A′	σ_{17}X	23,793	−76.4	−52.4	−54.5
11.278	A″	σ_{17}Z	691	−60.7	−48.7	−124.3
11.397	A″	π_2X	6387	−92.1	−95.3	−77.5
11.407	A′	σ_{17}Y	14,624	−97.6	−140.5	−75.9
11.498	A′	σ_{17}S	24,687	−94.0	−70.8	−81.8
11.535	A″	σ_{17}YZ	10,643	−105.6	−162.1	−201.1
11.556	A′	σ_{17}X	2541	−265.6	−225.0	−181.6
11.563	A″	σ_{17}XZ	897	−109.9	−65.0	−137.2
11.631	A″	σ_{16}Z	3161	−47.3	−29.5	−66.2
11.639	A″	σ_{17}Z	155	−94.0	−66.2	−178.8
11.722	A′	π_2XZ	3434	−111.1	−69.6	−143.7
11.752	A″	π_2XY	4474	−112.4	−70.7	−72.2
11.768	A″	σ_{179}YZ	15,879	−99.9	−172.0	−204.0
11.810	A″	π_2Y	3628	−99.4	−147.5	−75.7
11.837	A′	π_2YZ	275	−86.6	−136.7	−163.5
11.914	A′	σ_{17}S	1789	−263.4	−220.1	−210.3
12.041	A″	π_2X	55,856	−80.5	−61.7	−57.7
12.067	A″	σ_{17}Z	4	−141.2	−123.1	−342.4
12.085	A″	π_2XY	503	−151.1	−93.6	−72.0
12.156	A″	σ_{17}Y	38	−110.3	−96.2	−260.9
12.173	A′	σ_{17}XY	6121	−86.8	−70.5	−53.7
12.309	A′	σ_{17}Y	10,223	−159.5	−264.2	−121.1
12.333	A″	π_2X	1138	−266.6	−229.6	−180.7
12.404	A′	σ_{16}Y	736	−62.1	−80.7	−53.1
12.473	A″	σ_{17}XZ	139	−250.3	−146.2	−313.2
12.831	A″	σ_{16}YZ	104	−65.5	−93.6	−120.7
13.010	A′	σ_{16}X	886	−81.3	−60.5	−60.8
13.030	A″	π_2Y	738	−154.8	−264.6	−117.9
13.336	A″	σ_{16}Z	268	−58.9	−49.5	−125.2
13.337	A″	σ_{16}XZ	343	−118.1	−71.4	−153.2
13.358	A′	σ_{16}XY	34,514	−120.0	−69.2	−77.6
13.407	A′	σ_{16}Y	1971	−97.3	−142.7	−76.9
13.568	A″	σ_{16}YZ	193	−123.7	−195.6	−240.8
13.573	A′	σ_{16}XY	25,895	−144.7	−90.5	−71.6
13.655	A″	σ_{16}YZ	698	−74.6	−132.6	−156.5
13.692	A″	σ_{16}XZ	1129	−85.5	−53.6	−124.1

[a] Relative to total energy −568.05969 a.u.

group. There do not appear to be experimental studies of triplet states for isothiazole.

4.2.2. Cationic states in the UV-PES assignment

Relative to the UV-PES, the adiabatic π-ionisation energy IE_A is high by ∼0.28 eV, while the difference in IE_A for the π- and σ-ionisations (0.67 eV) is smaller than $IE_V^1 - IE_V^3$ in the UV-PES data (1.1 eV), but this order of cationic states, $\pi_4^{-1} < \sigma_{18}^{-1}$, supports the previous assignment [11]. We are unable to generate a structure

for the second π-ionisation, owing to collapse of the structure to π_4^{-1} above.

The vertical study of IE_V by GF, TDA and CI methods (Table 2) also shows that π-ionisation is the lowest ionic state, in agreement with previous conclusions [24–28]. All the present methods, CI, TDA and GF (Table 2), give the sequential IE_V order: $\pi_4^{-1} < \pi_3^{-1} < \sigma_{18}^{-1} < \sigma_{17}^{-1}$, in agreement with previous studies [11,29–31]. We note that some previous authors have used valence shell numbering of orbitals. The Rydberg series reflect this order, as is discussed below.

4.2.3. The calculated valence state vertical excitation energies for isothiazole

Some 23 calculated valence states (Table 3) are predicted to lie in the spectral range 6–12.0 eV. The upper σ* states are often mixtures of significant VMOs, and we omit the separate terms in some cases. The main oscillator strength arises from A′ states, in which several ππ* and σσ* states are intense. Seven A′ bands have oscillator strength $f(r) > 0.1$, and several of these occur as linear combinations. The strongest bands with $f(r)$ are: $\pi_4\pi_6^* + \pi_3\pi_5^*$ (0.28) and $LP_S\sigma_{20}^* - LP_S\sigma_{19}^*$ (0.28). These are followed by $\pi_3\pi_6^* + \pi_2\pi_5^*$ (0.23); $\pi_4\pi_5^* + \pi_3\pi_6^*$ (0.21), $\pi_3\pi_5^* - \pi_4\pi_6^*$ (0.12); $LP_N\sigma_{20}^* - LP_N\sigma_{19}^* + \pi_3\pi_6^*$ (0.15); $\pi_2\pi_5^*\,\pi_3\pi_6^* - \pi_3^0\pi_5^{2*}$ (0.11). The last example shows a considerable contribution from a doubly excited state.

The positions of these intense bands and their groupings can be correlated with the most prominent maxima of the spectrum (Fig. 9); the theoretical energies have been increased by 0.14 eV, to give a closer fit, justified by the much larger CI dimensions of the excited states in relation to the ground state. Thus the lowest band at ~5.2 eV is probably a single ππ* excitation together with an $LP_N\pi^*$ state, which is calculated between the first two bands. The broad band between 5.7 and 6.5 eV probably contains four valence states; the strongest is again ππ*, but with $LP_N\sigma^*$ (medium) and $\pi_4\sigma^*$ and $\pi_3\sigma^*$ (very weak). The region 7–8.5 eV also appears to contain five valence states (Table 3), one of which is very weak ($LP_N\pi^*$). This band again is

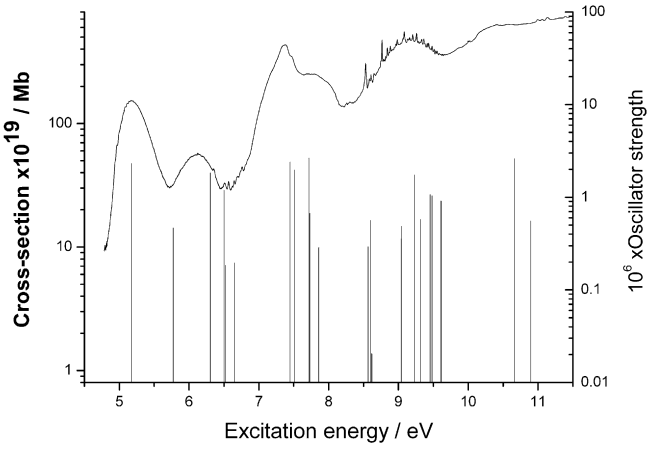

Fig. 9. The calculated valence states superimposed on the VUV spectrum.

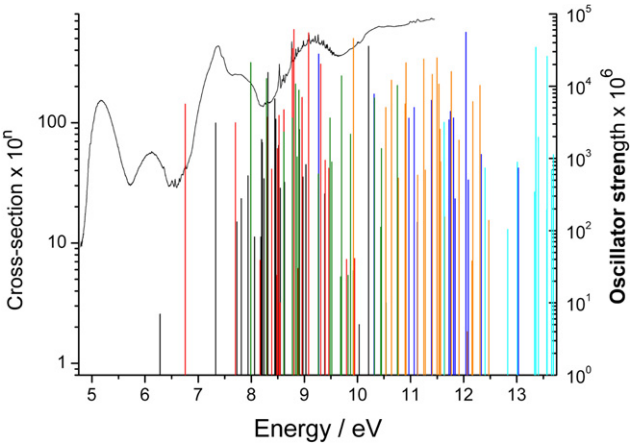

Fig. 10. The calculated Rydberg states superimposed on the VUV spectrum.

dominated by ππ* excitations, together with a very strong $LP_N\sigma^*$. The 8.5–10 eV envelope correlates with a number of calculated valence states, which probably have the lower intensity of the Rydberg states superimposed.

4.2.4. The calculated Rydberg state vertical excitation energies for isothiazole

Comparisons with experiment are given in Section 5 below; here we refer to the theoretical manifold (Table 5, Fig. 10) in isolation. In the studies of Rydberg states, all potential vacating MOs were symmetrically treated in terms of CSF; thus excitations involving π_4, π_3 and π_2 were treated equivalently, as were those involving σ_{18} (LP_N), σ_{17} (LP_S) and σ_{16}. In practice, individual Rydberg roots were generally dominated by a single π- or σ-occupied MO (the lower state), which contrasts with those involving π_4 and π_3 in ππ*-valence excitations, where mixing frequently occurred. For simplicity we retain usage of S, X, Y, Z, XY, XZ, YZ, etc. in this section.

The lowest calculated Rydberg states were $\pi_4$3S and $\pi_3$3S, with a separation of 0.475 eV. Both these calculated states both have $\delta = 1.02$; the second moment terms, although non-spherical, are consistent with 3s states [1–8]. The present calculations suggest that the observed p-states (X, Y, Z) could show considerable splitting, since the calculated values have $\pi_4$3Y differing from $\pi_4$3X and $\pi_4$3Z by ~0.5 eV; similarly for the roots involving $\pi_3$3Y + $\pi_3$3Z; however, the intensity of the Y-states is markedly higher than those involving X- and Z-Rydberg states. The separation of $\pi_4$3Y and $\pi_3$3Y by ~0.5 eV is also consistent with the s-states above. The next two higher calculated states ($\pi_4$4S and $\pi_4$3YZ) are very close, as expected, but differentiated by $\delta = 1.18$ ($n = 4$) and 0.18 ($n = 3$), respectively. A group of A″ valence states (πσ* 8.21, 8.77, 10.88 eV) occur within the Rydberg root sequence, and these can be expected to have a perturbing effect upon neighbouring Rydberg states of same symmetry.

4.2.5. Variation in calculated Rydberg state excitation energies with originating MOs

Recently, we showed [39] that the systematic differences between corresponding upper states in the calculated Rydberg series for but-2-yne, give a measure of the differences between the corresponding lower states, and hence the IE involved. This provided a further assignment check for the IE. A comparison of π_4- and π_3-calculated Rydberg states (17 in total), where the upper state is identical (nS, nP or nD), shows a fairly tight correlation between the two sets of data (slope 0.986, with standard deviation (SD) 0.121 eV). Overall this shows that the relative values of the members of the sequence are consistent. The median difference between corresponding members of the two series (0.42 eV), is larger than the IE_V difference (0.25 eV), as mentioned above for the $\pi_4$3S and $\pi_3$3S states. In a similar manner, we can correlate the upper states for all other originating MOs. These should then correlate with the relative IE of the lower states. For the following sequences we have median difference (MD) (eV) between pairs of orbitals, with SD in parentheses: π_4–π_3 0.42 (0.24); π_4–π_2 3.2 (0.23); π_4–σ_{18} (LP_N): 1.4 (0.41); π_4–σ_{17} (LP_S): 3.2 (0.32). Thus, we arrive at calculated IE differences from IE_1 of 0.42 (π_3), 1.4(LP_N), 3.2 (π_2) and 3.2 (LP_S). This aspect of the Rydberg state

Table 6
Ground state atomic and molecular properties for isothiazole compared with experiment, at equilibrium structures

Property	Spectral data	cc-pVTZ B3LYP	cc-pVTZ MP2	TZVP B3LYP	TZVP MP2
Energy/a.u.		−569.14606	−568.34620	−569.12530	−568.19197
A/MHz	8275.59 [15]	8261.97	8376.38		8247.44
B/MHz	5846.25 [15]	5821.45	5905.22		5779.01
C/MHz	3424.20 [15]	3415.13	3463.50		3398.01
Dipole moment					
μ_{total}/D	2.39 [12]	2.399	2.315	2.575	2.465
μ_A/D	1.12 [12]	1.094	0.947	1.129	0.942
μ_B/D	2.11 [12]	2.134	2.112	2.314	2.278
$\theta_{\mu A}$/°	62.0	62.8	65.9	64.0	67.5
^{14}N quadrupole coupling/MHz					
χ_{aa}	1.037 (23) [12] 1.0732 (47) [13]	1.036	1.010	1.153	1.125
χ_{bb}	−2.404 (27) [12] −2.4753 (46) [13]	−2.620	−2.398	−2.435	−2.243
$\chi_{cc} = \chi_{xx}$	1.367 (27) [12] 1.4021 [13]	1.584	1.387	1.281	1.118
χ_{ab}	−	3.092	2.726	3.198	−2.871
η_{1A}	0.137	0.209	0.157	0.054	0.003
χ_{yy}		2.800	2.521	3.026	2.769
χ_{zz}		−4.384	−3.909	−4.307	−3.887
η_{PA}		0.277	0.290	0.405	0.425
θ_{zzA}		−60.29	−60.86	−59.65	60.20
^{33}S quadrupole coupling/MHz					
χ_{aa}	8.7015 (57) [13]	8.924	9.614	6.394	7.617
χ_{bb}	−32.9696 (60) [13]	−28.798	−26.564	−30.141	−27.506
$\chi_{cc} = \chi_{yy}$	24.2681 [13]	19.874	16.950	23.747	19.888
χ_{ab}	−	−4.865	−4.985	−5.214	5.315
η_{1A}	0.5824	0.380	0.276	0.576	0.446
χ_{xx}		9.541	10.289	7.123	8.404
χ_{zz}		−29.415	−27.238	−30.871	−28.292
η_{PA}		0.351	0.245	0.538	0.406
θ_{zzA}		82.77	82.30	82.04	81.58
Quadrupole moment/10^{-26} esu cm^2					
Q_{aa}	5.1 (6) [32]	4.476	4.580	4.916	5.007
Q_{bb}	0.0 (6) [32]	−0.149	−0.239	−0.469	−0.685
$Q_{cc} = Q_{yy}$	−5.1 (10) [32]	−4.327	−4.341	−4.447	−4.323
Q_{ab}	−	2.242	2.127	2.372	−2.228
Q_{xx}		−1.058			
Q_{zz}		5.385			
θ_{zzA}		22.06			
Second moments/10^{-16} cm^2					
$\langle a^2 \rangle$	54.4 (22) [32]	54.74	54.08	55.29	55.13
$\langle b^2 \rangle$	42.0 (22) [32]	42.29	41.89	42.73	42.58
$\langle c^2 \rangle$	8.0 (22) [32]	7.94	7.97	8.01	8.07

manifold establishes the IE order as: $\pi_4 < \pi_3 < LP_N < \pi_2 \sim LP_S$, and is the same sequence as that determined by the CI study of vertical ionic states above (Table 2).

4.2.6. The calculated triplet state vertical excitation energies

Comparison of the results in Tables 4 and 6 shows that the triplet states are generally less complex mixtures of leading CSF. Two triplets of $\pi\pi^*$ type and one $LP_N\pi^*$ occur about 1 eV below the corresponding singlets. The ^1S–^3T separation is rather less for the $\pi\sigma^*$ states at ~0.5 eV. In the absence of experimental triplet state results, we suspend further comment on this issue.

5. Comparison of the calculated valence and Rydberg manifolds with the experimental VUV spectrum

Super-position of the calculated Rydberg state intensities and the VUV envelope shows that the gross features of the experiment are reproduced. Thus, the small number of calculated Rydberg states in the 6–8 eV region, may be present as sharp bands on the broader valence transitions; higher members of the π_4nS series make such positioning inevitable, although such bands may not be observable in the current spectrum. These are followed by extensive Rydberg activity between 8 and 10 eV in the experiment, and replicated by the high density of calculated Rydberg states in that region. Because of the basis set and CI limitations above 10 eV, the number of calculated states is necessarily smaller, but this is accompanied with less obvious Rydberg activity in that region as well.

The separation of the lowest calculated Rydberg states $\pi_4$3S and $\pi_3$3S 0.475 eV, is slightly larger than the observed IE_V difference (0.25); we find $\delta = 1.02$ for these series, to be compared with 1.08 experimentally for higher members of the former. The experimental δ values (0.48 and 0.50) compare with 0.52 and 0.21 for $\pi_4$3X and $\pi_4$3Z, but 0.48 and 0.36 if the values relate to $\pi_4$3X and $\pi_3$3X; however, this requires that the vibrational structure of π_4- and π_3-ionisations are similar, and this is not yet known. We note that both IE_1 and IE_2 for the closely related isoxazole (Fig. 1, **2a**) have high 0–0 bands, and hence possibly related structure, but IE_2 is not fully resolved from IE_3 either.

6. Conclusions

The VUV spectrum of isothiazole has been reported for the first time. Comparison with the calculated results for Rydberg states is difficult, since only a few series were apparent in the experimental spectrum, and the low-lying members were not detected; such states are the only ones readily calculated. It is clear that valence states are important in the intensity distribution of the VUV spectrum, both at low excitation energy, and elsewhere in the spectrum. These conclusions are supported by *ab initio* multi-reference multi-root CI calculations, which yield seven valence states with high intensity ($f(r) > 0.1$). All of the most intense calculated bands are of A′ symmetry.

The two lowest UV bands certainly are dominated by $\pi\pi^*$ excitation from both of the higher π-orbitals (π_4 and π_3), which occur as symmetric and antisymmetric combinations, with $\pi_4\pi_5^* + \pi_3\pi_6^*$ followed by $\pi_3\pi_5^* - \pi_4\pi_6^*$. The second band also includes states which are heavily localised on N (both $LP_N\pi^*$ and $LP_N\sigma^*$).

With the exception of the A′ state $LP_N\sigma_{20}^* - LP_N\sigma_{19}^* + \pi_3\pi_6^*$, most of the valence excitations from LP_N were weak in intensity; however, a similar A′ state $LP_S\sigma_{20}^* - LP_S\sigma_{19}^*$ is among the most intense, even though it lies at high energy. Double excitation CSF do not contribute as leading terms below about 9.5 eV, but examples such as $\pi_3^0\pi_5^{2*}$ and $\pi_3\pi_4\pi_5^{2*}$ have significant density above that region.

The significant mixing of $\pi\pi^*$ states is striking, and is more reminiscent of the situation in benzene, where the equivalent situation is $\pi_2\pi_4^* \pm \pi_3\pi_5^*$, than to most of the previous heterocycles studied in these papers [1–8]; this suggests that there is more interaction between the π- and π*-MOs than for most compounds of this series [1–8], and this may possibly be an indicator of higher aromatic character.

Analysis of the VUV spectrum in detail has led to the identification of a considerable number of Rydberg states, but most of these are members of just three series, which reduces the possibility for comparison with the theoretical values. Estimates of the positions of numerous Rydberg states derived from the lowest group of six IE, comprising π_4 to π_2 and σ_{18} (LP_N), σ_{17} (LP_S) and σ_{16} are given.

The most intense Rydberg states found in the calculations are π_4Z and π_4YZ; excitations from π_3 and π_2 are generally less intense, but again π_3Z and π_3YZ are notable. In contrast, the most intense calculated values for σ-Rydberg excitations are s- and d_{xy}-states, i.e., $\sigma\sigma^*$ excitations.

The adiabatic structures of the lowest cationic states of A′ and A″ symmetry were determined. The lowest triplet state was found to be non-planar with the $\pi\pi^*$ (A′) state being a saddle point. These three structures when compared with the ground state showed a considerable change in the classical C=C–C=C unit towards C–C=C–C as well as changes involving the S-atom.

The Rydberg state calculations, using energy differences between excitations from differing MOs to similar upper states, support the early assignment [11] of the UV-PES spectrum as $\pi_4^{-1} < \pi_3^{-1} < \sigma_{18}^{-1}(LP_N) < \sigma_{17}^{-1}(LP_S) \sim \pi_2^{-1} < \sigma_{16}^{-1}$.

Acknowledgements

We thank the Daresbury Laboratory (DL) for an award of SRS beam-time; the assistance of, and helpful discussions with, Drs. D.M.P. Holland and D.A. Shaw (DL). We also thank: the Edinburgh Parallel Computing Centre (EPCC) for computing facilities; Drs. M.F. Guest and P.

Sherwood (DL) for maintenance and development of the GAMESS-UK suite of programmes.

Appendix A. Electronic ground state properties of isothiazole

A summary of experimental and the present theoretical data (Table 6), shows comparisons of B3LYP density functional, and electron correlated MP2 calculations for the basis sets used in parts of the present study. All the present results are relatively in close agreement with MW experiments [12,13,32]; the numerically best values are cc-pVTZ+B3LYP. The normal convention of quadrupole moment (QM) magnitudes: $Q_{zz} \geqslant Q_{yy} \geqslant Q_{xx}$ is used; similarly, the electric field gradients (EFG) which generate the ^{14}N and ^{33}S quadrupole coupling constants (QCC) have $\chi_{zz} \geqslant \chi_{yy} \geqslant \chi_{xx}$ in magnitudes. The two asymmetry parametera for inertial axes (η_{IA}) and principal axes (η_{PA}) are respectively defined as $(\chi_{bb} - \chi_{cc})/\chi_{aa}$ and $(\chi_{yy} - \chi_{xx})/\chi_{zz}$. We give the IA data for QM and QCC, including the only non-zero off-diagonal elements (Q_{ab} and χ_{ab}) for direct comparison with MW (a, b, c) data; the principal axis (PA; x, y, z) data obtained by diagonalization of the 3×3 (strictly 2×2 plus 1×1) matrices, gives the chemically more significant PA data. The angles between the PA systems and the IA axes are shown ($\theta_{\mu A}$, θ_{zzA}). The atomic quadrupole moments (Q_{Nucl}), which linearly scale the calculated electric field gradients (EFG) to QCC, follow recent recommendations [33,34]. The overall atomic and molecular properties, in terms of directions are shown in Fig. 11, while the magnitudes in both the IA and PA axes are shown in Table 6.

(a) *The dipole moment components*: The dipole moment lies perpendicular to the C_4C_5 bond, with its negative end towards N_2 (Fig. 9); it is clearly rotated from the $C_3N_2S_1$ angle bisector, towards S_1.

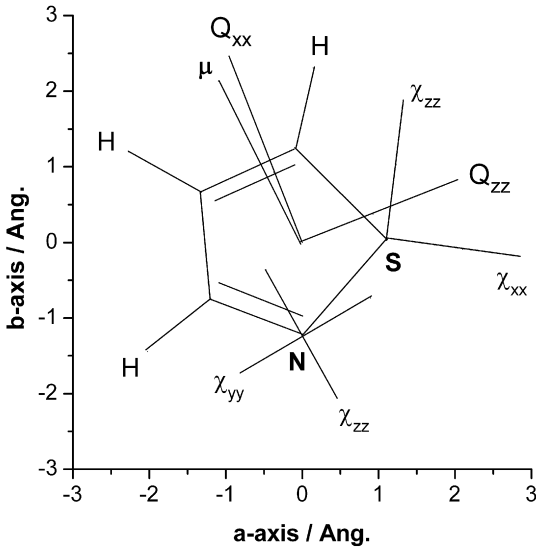

Fig. 11. The ground state molecular properties, using the B3LYP results.

(b) *The second moment components*: All the present values for both molecular quadrupole moments (Q_{ii}) and the second moments of the charge distribution ($\langle rr \rangle$ where r is a, b or c, as in the inertial axes), are in reasonable (Q_{ii}) or good accord ($\langle rr \rangle$) with experiment; the experimental error bars for Q_{ii} are large, as is usual. The present studies can be expected to give reliable values for the off-diagonal values (Q_{ab}, $\langle ab \rangle$) which are not determined experimentally. The principal value (Q_{zz}) lies relatively close to the *a*-axis.

(c) *The ^{14}N and ^{33}S nuclear quadrupole coupling constant (NQCC) components*: The ^{14}N value of χ_{zz} (close to −4.3 MHz) is typical of LP_N values [35], but is not directly available from the MW IA data; a large positive value for χ_{yy} is also typical of the large π-component values in heterocycles [35].

The ^{33}S results show that the PA and IA value identity is $\chi_{zz} \equiv \chi_{bb}$, but the numerical agreement of the four sets of results (Table 6) is not as good as is usually obtained, and this is surprising [36]; χ_{cc} is significantly larger than in thiophene (20.9525 (47) [37]) or thiazole (19.0041 (130) [38]), and this is the only term which is invariant to the axis system; whether this is a feature of the S–N bonded nature of isothiazole is unclear, and there are few related molecules.

Appendix B. The data collection and instrumental arrangement

The sample gas entered the absorption flow cell through a fine needle valve positioned centrally between the two LiF windows (25.6 cm). Synchrotron radiation from the Daresbury Laboratory storage ring which delivers radiation over a photon energy range of 5–40 eV has been described in detail previously [17]. The 5 m normal incidence monochromator employed had a photon resolution of 0.1 nm FWHM (~5 meV at $h\upsilon = 8$ eV). The radiation leaving the monochromator exit slit entered a chamber containing a 2:1 demagnifying ellipsoidal mirror, which was focussed on a position close to the LiF window at the entrance to the absorption cell. After passing through the second LiF window, the radiation entered an evacuated region (~25 cm), before impinging upon a sodium salicylate screen sprayed upon a glass window. The resulting fluorescence passed through a blue Kodak Wratten 47B filter, removing the long wavelength scattered light, before being detected with a photomultiplier. The evacuated region separates the gas sample from the sodium salicylate screen, thereby ensuring that the fluorescence efficiency was not affected by surface reactions. The pressure was measured using a 0–1 Torr capacitance manometer (MKS baratron, type 390 HA). The baratron is designed to operate at an elevated temperature of 45 °C. Thermal transpiration effects between the absorption cell and the sensor assembly need to be taken into consideration to be certain that the correct pressure is being recorded [18,19]. The entire apparatus was placed in a thermostatically controlled insulated

box, which was maintained slightly below 45° to enable the baratron to regulate properly.

The absolute photoabsorption cross section was obtained through application of the Beer–Lambert law [20], $I_t = I_0\exp(nl\sigma)$, where I_t is the intensity of the transmitted radiation after passing through the gas column, I_0 is the corresponding incident intensity, n is the gas number density, σ is the photoabsorption cross section and l is the length of the gas column. To determine σ as a function of photon energy, the monochromator was stepped over the chosen energy range; at each step readings proportional to I_t and the electron beam current in the storage ring (as well as the baratron pressure) were recorded. The entire procedure was then repeated with the empty cell to obtain I_0. For the present measurements on isothiazole, photoabsorption spectra were recorded using gas pressures in the 20–50 μbar range. The experimental uncertainty associated with the determination of absolute photoabsorption cross sections using this cell is estimated as ~5%.

To calibrate the photon energy scale, high resolution absorption spectra of a gas mixture comprising isothiazole, nitrous oxide and nitric oxide were recorded. The spectra of nitrous oxide and nitric oxide contain many sharp peaks, of well established photon energy, an hence this procedure enabled the photon energy scale of the spectrum of isothiazole to be calibrated.

References

[1] M.H. Palmer, I.C. Walker, C.C. Ballard, M.F. Guest, Chem. Phys. 192 (1995) 111.
[2] M.H. Palmer, I.C. Walker, M.F. Guest, Chem. Phys. 238 (1998) 179.
[3] M.H. Palmer, P.J. Wilson, Mol. Phys. 101 (2003) 2391.
[4] M.H. Palmer, I.C. Walker, M.F. Guest, Chem. Phys. 241 (1999) 275.
[5] M.H. Palmer, I.C. Walker, M.F. Guest, Chem. Phys. 247 (1999) 349.
[6] I.C. Walker, M.H. Palmer, M.-J. Hubin-Franskin, J. Delwiche, Chem. Phys. Lett. 367 (2003) 517.
[7] M.H. Palmer, M.F. Guest, Chem. Phys. 291 (2003) 287.
[8] I.C. Walker, M.H. Palmer, J. Delwiche, S.V. Hoffmann, P.L. Vieora, N.J. Mason, M.F. Guest, M-J. Hubin-Franskin, J. Heinesch, A. Giuliani, Chem. Phys. 297 (2004) 289.
[9] M.H. Palmer, G. Ganzenmuller, I.C. Walker, Chem. Phys. 334 (2007) 154.
[10] A. Garozzo, M.R. Pinizzotto, F. Guerrera, G. Tempera, A. Castro, E. GeremiaArchives of Virology Biomedical and Life-Sciences, vol. 135, Springer, 1994, 1-11; ISSN 1432-8798 (Online).
[11] M.H. Palmer, R.H. Findlay, J.N.A. Ridyard, A. Barrie, P. Swift, J. Mol. Struct. 39 (1977) 189.
[12] J.H. Griffiths, A. Wardley, V.E. Williams, N.L. Owen, J. Sheridan, Nature 216 (1967) 1301.
[13] J. Gripp, U. Kretschmer, H. Dreizler, Z. Naturforsch. 49A (1994) 1059.
[14] U. Kretschmer, Ber. Bunsen-Gesellschaft 99 (1995) 891.
[15] F. Hegelund, R. Wugt Larsen, R.A. Aitken, M.H. Palmer, J. Molec. Struct. 780–781 (2006) 45.
[16] G. Schultz, I. Hargittai, P. Friedman, J. Molec. Struct. 176 (1988) 61.
[17] D.M.P. Holland, J.B. West, A.A. MacDowell, I.H. Munro, A.G. Beckett, Nucl. Instrum. Methods B44 (1989) 233.
[18] L.B. Loeb, The Kinetic Theory of Gases, Dover, New York, 1961.
[19] K.F. Poulter, M.-J. Rodgers, P.J. Nash, T.J. Thompson, M.P. Perkin, Vacuum 33 (1983) 311.
[20] J.A.R. Samson, Techniques of Vacuum Ultraviolet Spectroscopy, Wiley, New York, 1967.
[21] A.D. McLean, G.S. Chandler, J. Chem. Phys. 72 (1980) 5639.
[22] R. Ahlrichs, P.R. Taylor, J. Chim. Phys. 78 (1981) 315.
[23] M.F. Guest, I.J. Bush, H.J.J. Van Dam, P. Sherwood, J.M.H. Thomas, J.H. Van Lenthe, R.W.A. Havenith, J. Kendrick, Mol. Phys. 103 (2005) 719.
[24] R.J. Buenker, in: P.G. Burton, (Ed.), Proceedings of the Workshop on Quantum Chemistry and Molecular Physics, Woolongong Univ. Press, 1980.
[25] R.J. Buenker, in: R.J. Bartlett (Ed.), Studies in Physical and Theoretical Chemistry, Elsevier, Amsterdam, 1982.
[26] R.J. Buenker, R.A. Phillips, J. Mol. Struct. (Theochem) 123 (1985) 291.
[27] S. Krebs, R.J. Buenker, J. Chem. Phys. 103 (1995) 5613.
[28] M.H. Palmer, J. Mol. Struct. 834–836 (2007) 113.
[29] G. Salmona, Y. Ferre, E.J. Vincent, Compt. Rend. Serie C: Sci. Chim. 273 (1971) 863.
[30] G. Salmona, Y. Ferre, E.J. Vincent, D. Megy, J. Chim. Phys. Phys. Chim. Biol. 69 (1972) 1292.
[31] G. Salmona, R. Faure, E.J. Vincent, C. Guimon, G. Pfister-Guillouzo, J. Mol. Struct. 48 (1978) 205.
[32] J. Wiese, D.H. Sutter, Z. Naturforsch. 35A (1980) 712.
[33] P. Pyykko, Z. Naturforsch. 47A (1992) 189.
[34] P. Pyykko, Mol. Phys. 99 (2001) 1617.
[35] M.H. Palmer, The calculation of electric field gradients by *ab initio* methods, and their relationship to experimental nuclear quadrupole coupling constants, Electronic Encyclopaedia of Computational Chemistry, Wiley, Chichester, UK, pp. 1–39.
[36] M.H. Palmer, Z. Naturforsch. 47A (1992) 203.
[37] U. Kretschmer, W. Stahl, H. Dreizler, Z. Naturforsch. 48A (1993) 733.
[38] U. Kretschmer, H. Dreizler, Z. Naturforsch. 48A (1993) 1219.
[39] M.H. Palmer, I.C. Walker, Chem. Phys., doi:10.1016/j.chemphys.2007.08.020.